Electronic Supplementary Material (ESI) for Nanoscale.
This journal is © The Royal Society of Chemistry 2024

Supplementary Information

Energetic MOF-derived Fe_3C nanoparticles encased in N, S-codoped mesoporous pod-like carbon nanotubes for efficient oxygen reduction reaction

Yang Liu, Xinde Duan, Fayuan Ge, Tingting Wu and Hegen Zheng*

State Key Laboratory of Coordination Chemistry, School of Chemistry and Chemical Engineering, Collaborative Innovation Center of Advanced Microstructures, Nanjing University, Nanjing 210023, P. R. China.

*Corresponding authors. *E-mail: zhenghg@nju.edu.cn (H. Zheng).*

Experimental section

All chemicals were used as received from commercial sources. ligand 4, 4′-bis(4-pyridyl)tetrazine (bptz) was synthesized following a reported procedure.[S1]

Material Characterization

Powder X-ray diffraction (PXRD) patterns were recorded on a Bruker D8 Advance X-ray diffractometer using Cu Kα radiation (λ = 1.5406 Å). Thermogravimetric analysis (TGA) was performed on a STA449F3 thermogravimetric analyzer at a heating rate of 10°C min^{-1} under N_2 gas flow. Raman spectra were recorded on a Invia Raman spectrometer using a 633 nm laser. Brunauer-Emmett-Teller (BET) specific surface areas were measured by N_2 physisorption on a Micromeritics ASAP 2050 system. Scanning electron microscope (SEM) was carried on a S-4800. Transmission electron microscope (TEM), high-resolution transmission electron microscope (HR-TEM), scanning transmission electron microscope (STEM) and elemental mapping were all collected on a JEOL JEM-2800 microscope. X-ray photoelectron spectra (XPS) analysis was carried out on a PHI-5000 Versa Probe XPS system. Inductively coupled plasma atomic emission spectrometry (ICP-AES) was measured on PerkinElmer Avio500 atomic emission spectrometer.

Electrochemical measurements

The ORR activity was evaluated by an electrochemical workstation (CHI 760E, Shanghai, Chenghua) in a standard three-electrode setup in 0.1 M KOH. A rotating disk electrode (RDE) can be used as the working electrode, Hg/Hg_2Cl_2 (KCl saturated) electrode and platinum electrode can serve as the reference electrode and counter electrode, respectively. All measured potentials are converted to reversible hydrogen electrode potential (E_{RHE}) using following Nernst equation: $E_{RHE} = E_{Hg2Cl2} + 0.2415 + 0.059pH$. The catalyst ink was prepared by ultrasonically dispersing the mixture of catalyst (5 mg), ethanol/H_2O solution (960 μL, 1/1, V/V), and Nafion (5 wt%, 40 μL) for 30 min. The catalyst dispersion (10 μL) was uniformly dropped onto a glassy carbon RDE (4 mm in diameter) and dried at room temperature.

Cyclic voltammograms (CV) measurements were performed at a scan rate of 10 mV s^{-1} in O_2- and N_2-saturated 0.1 M KOH solution, respectively. Linear sweeping

voltammetry (LSV) was tested in O_2-saturated 0.1 M KOH at a rotating rate ranging from 400 to 1600 rpm with a scan rate of 10 mV s^{-1}. The Tafel curve, derived from the LSV data, was represented by the equation η = a + b×log(j). In this equation, η stands for overpotential, b signifies the Tafel slope, and a indicates the intercept. The stability test was carried out by current versus time (i-t) chronoamperometric response at the half-wave potential ($E_{1/2}$) for 30000 s. The electrochemical surface areas (ECSA) can be estimated according to the double-layer capacitance (C_{dl}) values by recording cyclic voltammetry (CV) curves at different scan rates of 20, 40, 60, 80, 100, mV s^{-1} from 0.95 to 1.05 V (*vs.* RHE).

Rotating ring-disk electrode (RRDE) measurement was performed to further verify electron transfer number (n) and the production of peroxide yields (HO_2^-%) via following equations (Eq. S1- S2):

$$n = 4 \times \frac{I_d}{I_d + I_r/N} \quad \text{(Eq. S1)}$$

$$HO_2^- \% = 200 \times \frac{I_r/N}{I_d + I_r/N} \quad \text{(Eq. S2)}$$

Where I_d and I_r represent disk and ring current, respectively, and N represents the collection efficiency of the Pt ring (0.37).

Catalytic mechanism

Reaction mechanism of ORR in alkaline media

Reaction	Overall reaction	Reaction mechanism
ORR	$O_2 + 2H_2O(l) + 4e^- \rightarrow 4OH^-(aq)$	$* + O_2(g) + H_2O(l) + e^- \rightarrow HOO^* + OH^-(aq)$
		$HOO^* + e^- \rightarrow O^* + OH^-$
		$O^* + H_2O(l) + e^- \rightarrow HO^* + OH^-(aq)$
		$HO^* + e^- \rightarrow OH^-(aq) + *$

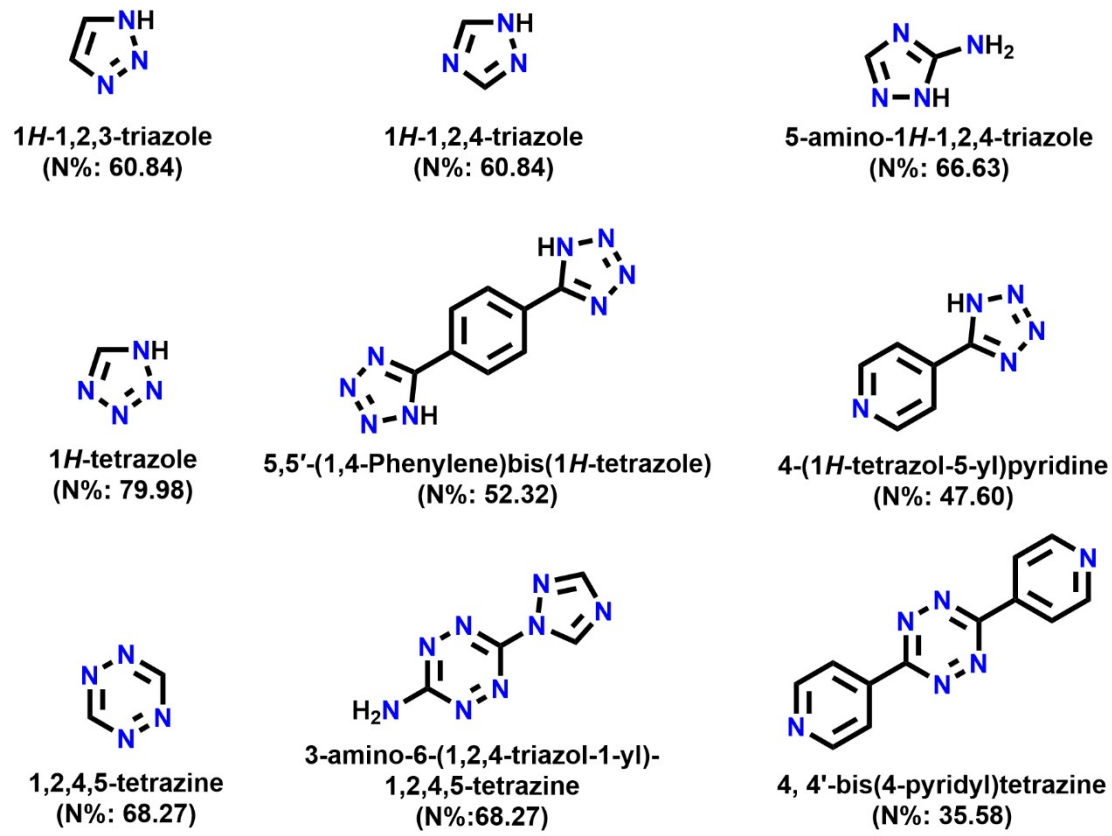

Scheme S1 Some examples of triazole, tetrazole and tetrazine and their derivatives.

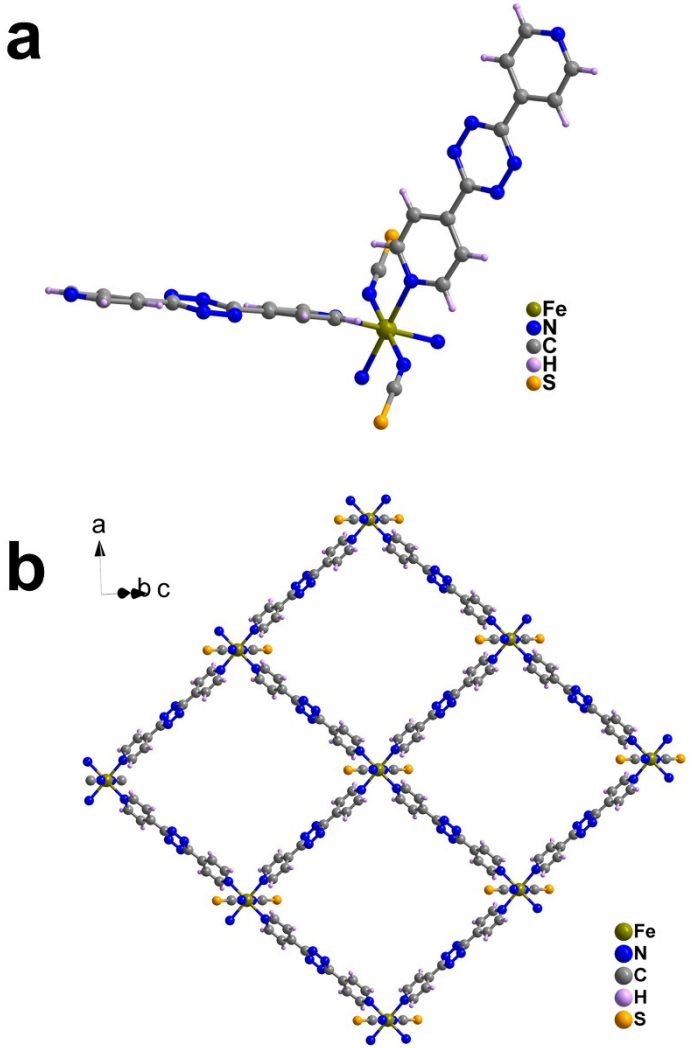

Fig. S1 (a) The asymmetric unit and (b) 2D network structure of Fe-EMOF.

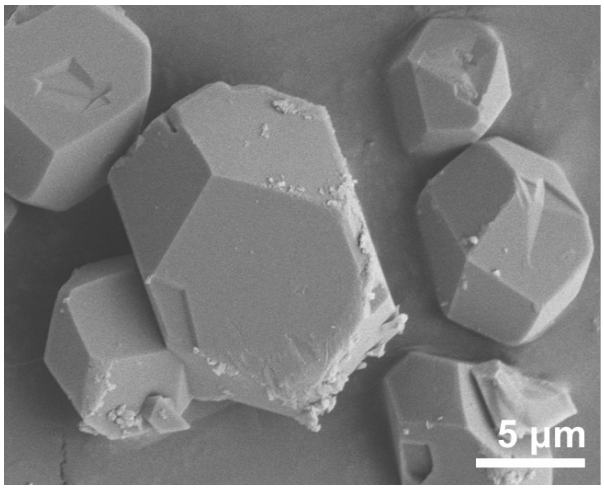

Fig. S2 SEM image of Fe-EMOF.

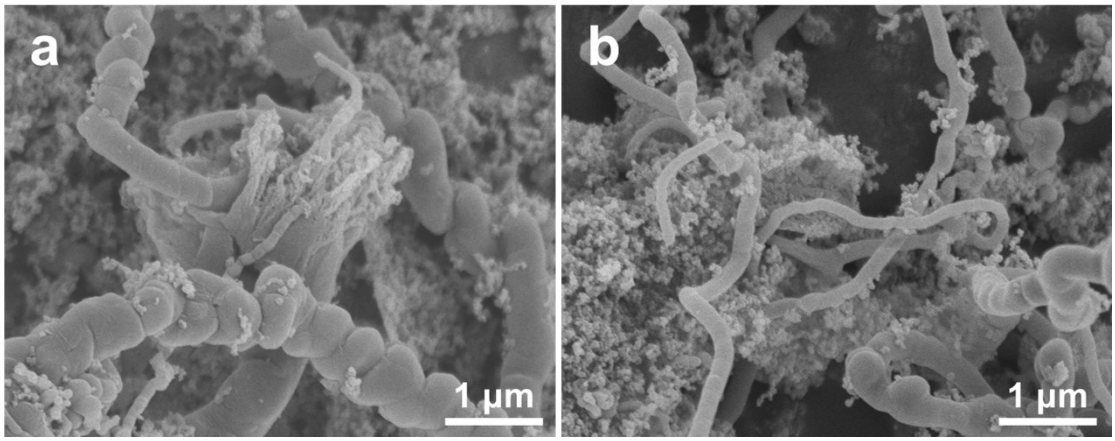

Fig. S3 SEM images of (a) Fe_3C@NSC-800, (b) Fe_3C@NSC-1000.

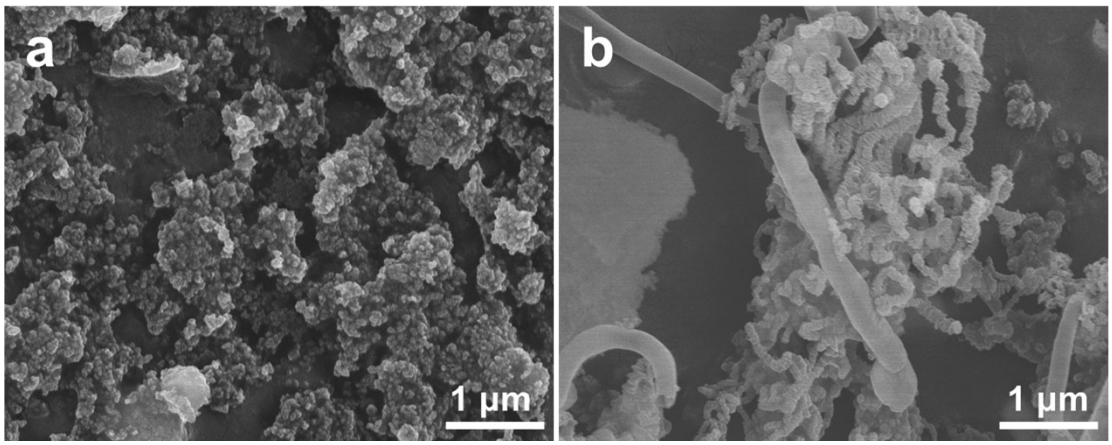

Fig. S4 SEM images of (a) Fe/KB-900 and (b) Fe/MA-900.

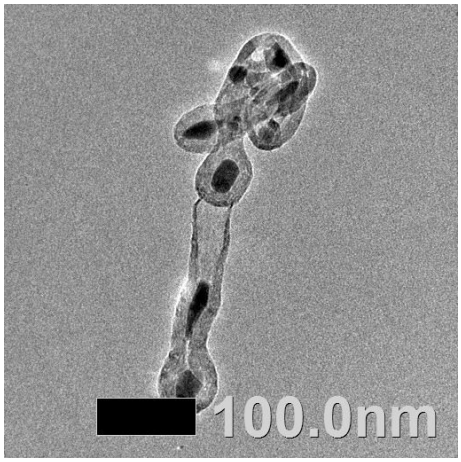

Fig. S5 TEM image of carbon nanotube in Fe_3C@NSC-900.

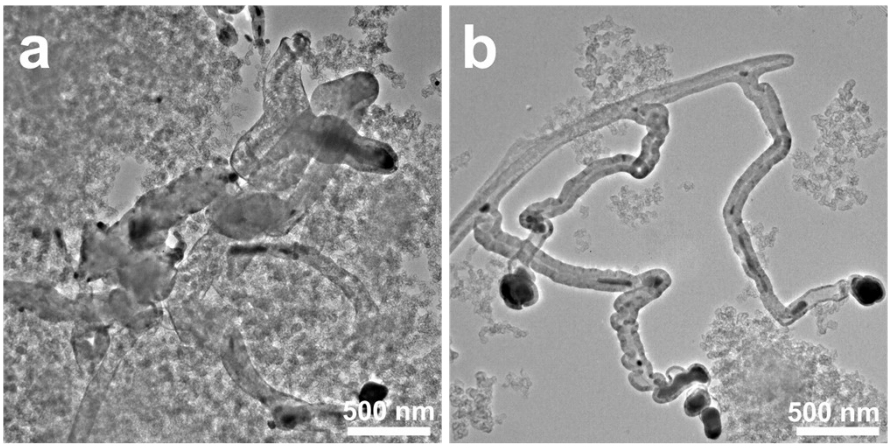

Fig. S6 TEM images of (a) Fe_3C@NSC-800, (b) Fe_3C@NSC-1000.

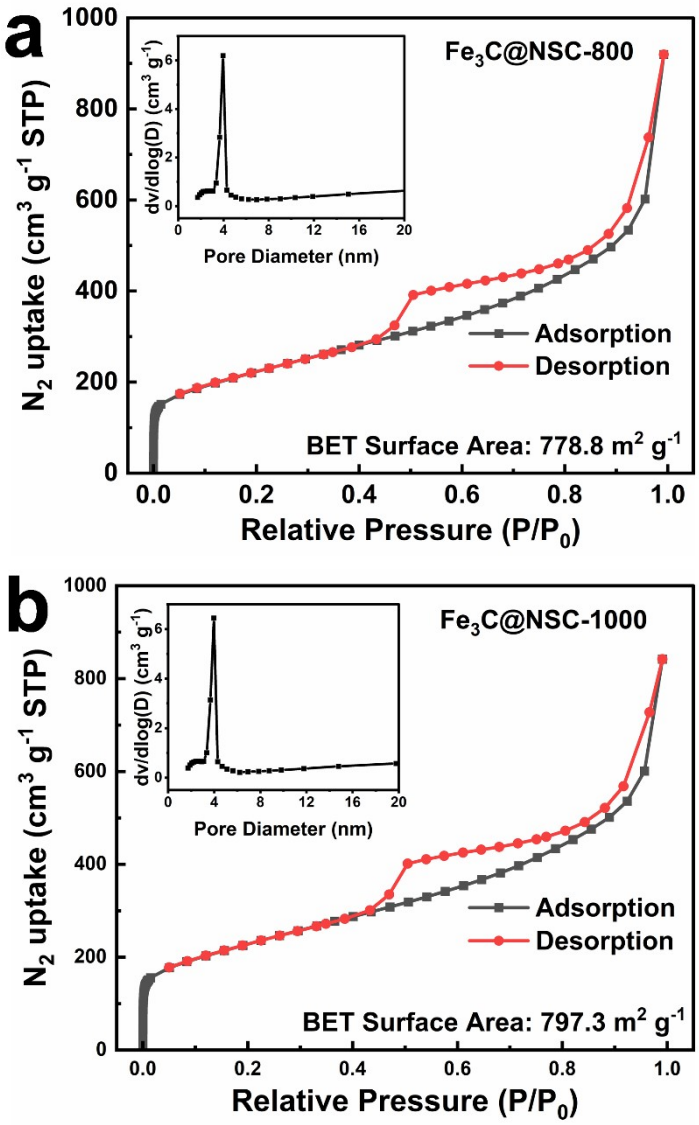

Fig. S7 N_2 adsorption-desorption isotherms and related pore size distributions for (a) Fe_3C@NSC-800 and (b) Fe_3C@NSC-1000.

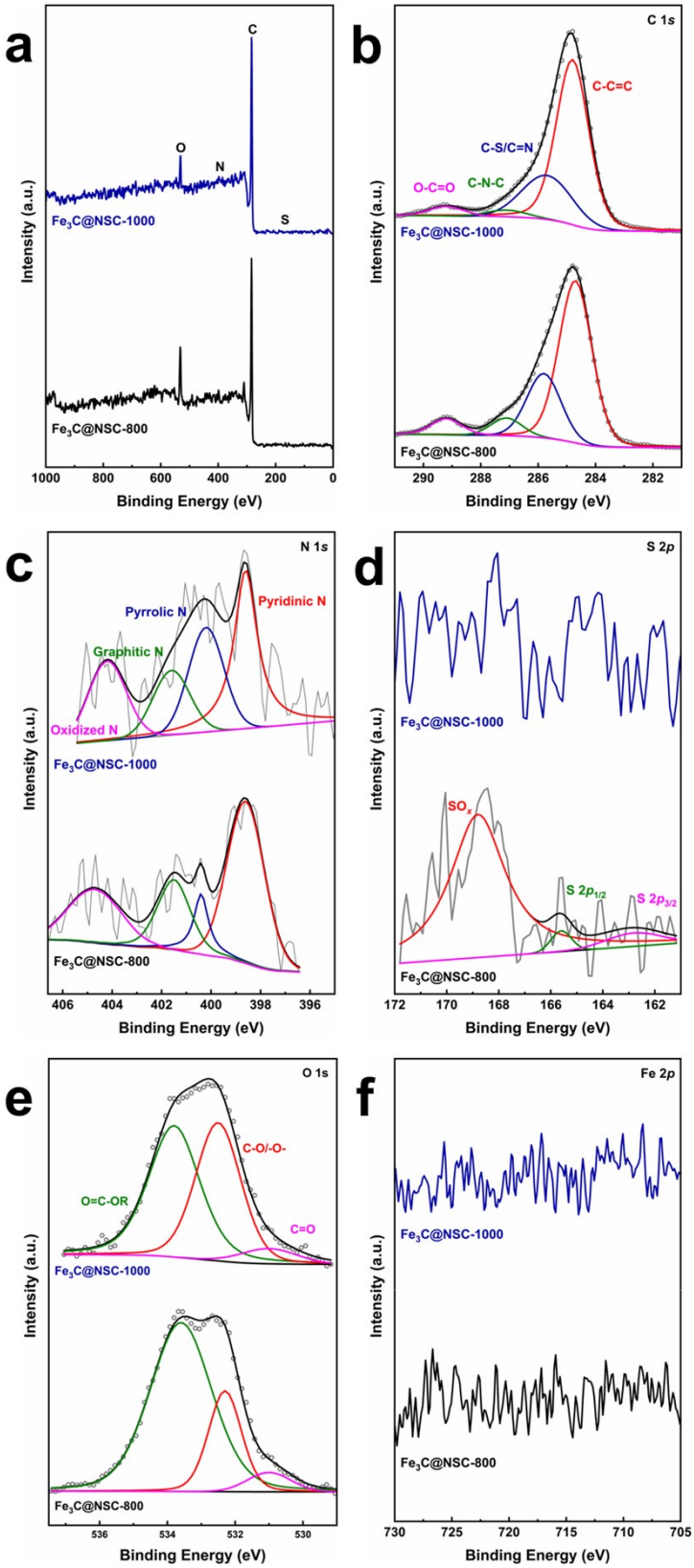

Fig. S8 (a) Survey XPS spectra; (b) C 1*s*; (c) N 1*s*; (d) S 2*p*; (e) O 1*s* and (f) Fe 2*p* high-resolution XPS spectra of Fe_3C@NSC-800 and Fe_3C@NSC-1000.

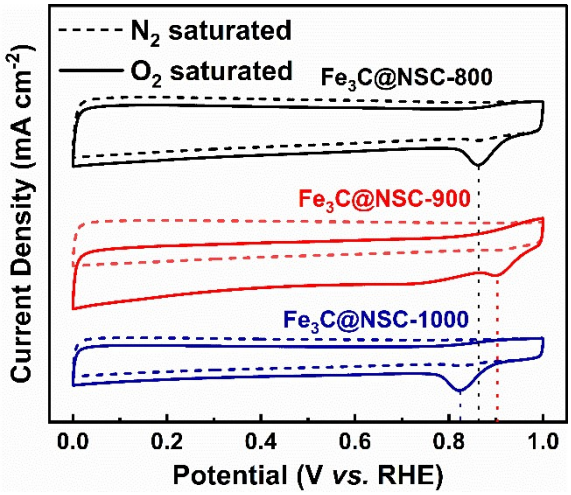

Fig. S9 CV curves of Fe_3C@NSC-T.

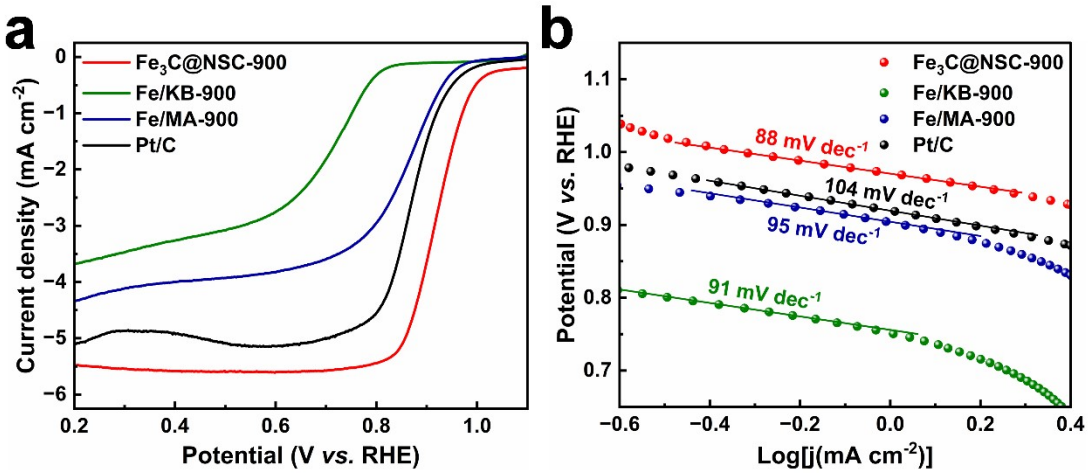

Fig. S10 (a) ORR polarization curves and (b) corresponding Tafel plots for Fe_3C@NSC-900, Fe/KB-900, Fe/MA-900 and Pt/C on RDE at 1600 rpm.

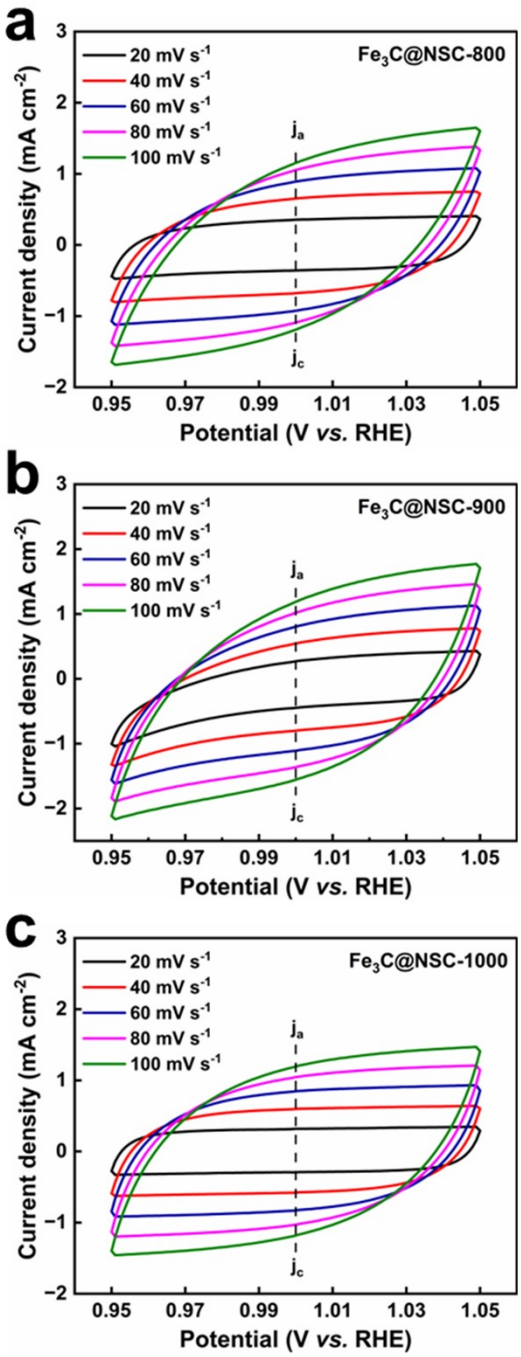

Fig. S11 (a-c) The cyclic voltammograms curves of Fe_3C@NSC-T in the region of 0.95-1.05 V vs. RHE in 0.1 M KOH.

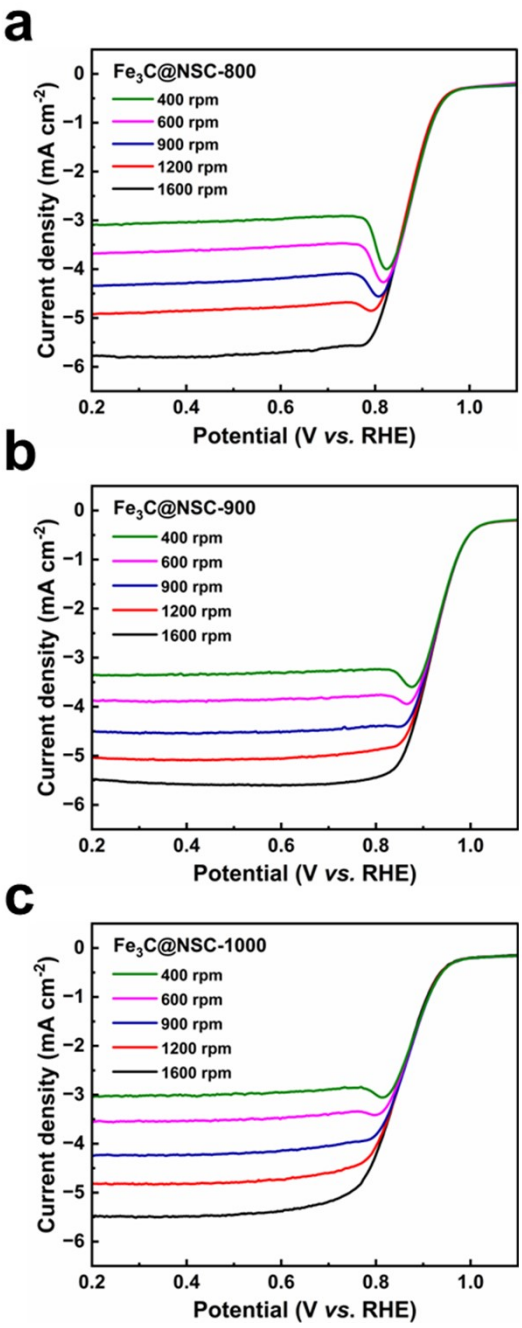

Fig. S12 (a-c) LSV curves of Fe_3C@NSC-T at various rotation speeds.

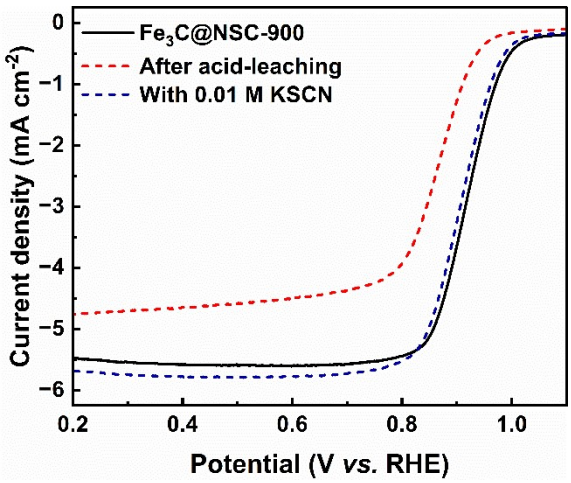

Fig. S13 LSV curves for ORR before and after acid-leaching and poisoning treatment with 0.01 M KSCN in 0.1 M KOH.

Table S1 XPS spectra analysis for samples.

Sample	C 1*s* (%)	N 1*s* (%)	O 1*s* (%)	S 2*p* (%)
Fe_3C@NSC-800	89.89	0.96	9.03	0.12
Fe_3C@NSC-900	95.64	0.86	3.35	0.14
Fe_3C@NSC-1000	94.29	0.76	4.95	--

Table S2 Corresponding contents of different N species for Fe_3C@NSC-T.

Sample	Pyridinic N	Graphitic N	Pyrrolic N	Oxidized N
Fe_3C@NSC-800	47.9%	20.1%	10.1%	21.9%
Fe_3C@NSC-900	54.0%	40.6%	3.3%	2.1%
Fe_3C@NSC-1000	37.5%	16.3%	25.2%	21.0%

Table S3 Summary of ORR performances of Fe_3C@NSC-900, 20% Pt/C and recently reported other advanced ORR catalysts under alkaline conditions.

Samples	Onset potential (E_0) (V *vs.* RHE)	Half-wave potential ($E_{1/2}$) (V *vs.* RHE)	Half-wave potential difference between the sample and Pt/C	Limiting current density (J_L) (mA cm^{-2})	Ref.
Fe_3C@NSC-900	1.177	0.922	0.052	5.480	This work
FeS/Fe_3C@Fe-N-C	0.99	0.91	0.031	-	S2
Fe@MET-M	-	0.895	0.027	4.909	S3
Fe_3C|Fe–N–C	0.982	0.888	0.035	5.165	S4
Fe_3C@NPW	-	0.87	0.020	5.19	S5
NC@Fe_3C-900	0.98	0.88	0.040	-	S6
Fe_{SA}/N,S-PHLC	0.97	0.91	0.031	-	S7
Fe/Fe_xC@Fe-N-C-900	1.01	0.91	0.050	5.72	S8
FeN_4-Fe_{NCP}@MCF	1.02	0.894	0.029	-	S9
Ni_3Fe-NCNTs-800	0.980	0.862	0.019	6.606	S10
$Fe_{SA/AC}$@HNC	0.99	0.90	0.040	-	S11

Co_{40}SAs/AC@NG	0.980	0.890	0.042	-	S12
FeCo-NSC	-	0.86	0.010	5.26	S13
$FeMn_{ac}$/Mn-N_4C	1.00	0.90	-	5.55	S14
FePc@CeO/NSCNF	1.00	0.89	0.030	-	S15
Co_1/Zn_{20}-N-C-200	-	0.89	0.020	5.78	S16
Ni,Fe-DSAs/NCs	-	0.895	0.030	-	S17
Co SAs/3D GFs	1.032	0.901	0.066	-	S18
Co,Zn SAs@Co-CNTs	1.02	0.92	0.05	-	S19
Co_2MnN_8/C	1.027	0.912	0.02	-	S20

References

S1. P. H. Dinolfo, M. E. Williams, C. L. Stern and J. T. Hupp, *J. Am. Chem. Soc.*, 2004, **126**, 12989-13001.

S2. S. Sun, F. Yang, X. Zhang, J. Qian, K. Wei, J. An, Y. Sun, S. Wang, X. Li and Y. Li, *Chem. Eng. J.*, 2024, **487**, 150673.

S3. G. Li, J. Liu, C. Xu, H. Chen, H. Hu, R. Jin, L. Sun, H. Chen, C. Guo, H. Li and Y. Si, *Energy Storage Mater.*, 2023, **56**, 394-402.

S4. Y. Chen, X. Kong, Y. Wang, H. Ye, J. Gao, Y. Qiu, S. Wang, W. Zhao, Y. Wang, J. Zhou and Q. Yuan, *Chem. Eng. J.*, 2023, **454**, 140512.

S5. M. Cao, Y. Liu, K. Sun, H. Li, X. Lin, P. Zhang, L. Zhou, A. Wang, S. Mehdi, X. Wu, J. Jiang and B. Li, *Small*, 2022, **18**, 2202014.

S6. J. Q.-Bermejo, A. Daouli, S. G. Dalí, Y. Cui, A. Zitolo, J. C.-Gutiérrez, M. Emo, M. T. Izquierdo, W. Mustain, M. Badawi, A. Celzard and V. Fierro, *Adv. Funct. Mater.*, 2024, **34**, 2403810.

S7. M. Yuan, Y. Liu, Y. Du, Z. Xiao, H. Li, K. Liu and L. Wang, *Adv. Funct. Mater.*, 2024, **34**, 2401484.

S8. M. Chen, F. Kong, H. Yao, Y. Chen, G. Meng, Z. Chang, C. Chen, H. Tian, L. Wang, X. Cui and J. Shi, *Chem. Eng. J.*, 2023, **453**, 139820.

S9. Z. Wang, Z. Lu, Q. Ye, Z. Yang, R. Xu, K. Kong, Y. Zhang, T. Yan, Y. Liu, Z. Pan, Y. Huang and X. Lu, *Adv. Funct. Mater.*, 2024, **34**, 2315150.

S10. Q. Yan, X. Duan, Y. Liu, F. Ge and H. Zheng, *J. Mater. Chem. A*, 2023, **11**, 1430-1438.

S11. H. Zhang, H.-C. Chen, S. Feizpoor, L. Li, X. Zhang, X. Xu, Z. Zhuang, Z. Li, W. Hu, R. Snyders, D. Wang and C. Wang, *Adv. Mater.*, 2024, **36**, 2400523.

S12. M. Zhang, H. Li, J. Chen, F.-X. Ma, L. Zhen, Z. Wen and C.-Y. Xu, *Adv. Funct. Mater.*, 2023, **33**, 2209726.

S13. Y. Wu, C. Ye, L. Yu, Y. Liu, J. Huang, J. Bi, L. Xue, J. Sun, J. Yang, W. Zhang, X. Wang, P. Xiong and J. Zhu, *Energy Storage Mater.*, 2022, **45**, 805-813.

S14. H. Liu, L. Jiang, J. Khan, X. Wang, J. Xiao, H. Zhang, H. Xie, L. Li, S. Wang and L. Han, *Angew. Chem. Int. Ed.*, 2023, **62**, e202214988.

S15. S. Tao, S. Xiang, Y. Yu, H. Lan, C. Liu and J. Zhang, *Carbon*, 2024, **220**, 118893.

S16. Y. Zhang, X. Yu Gao, Z. Wen, C. Cheng Yang and Q. Jiang, *Chem. Eng. J.*, 2022, **446**, 137441.

S17. Z. Wang, X. Jin, R. Xu, Z. Yang, S. Ma, T. Yan, C. Zhu, J. Fang, Y. Liu, S.-J. Hwang, Z. Pan and H. J. Fan, *ACS Nano*, 2023, **17**, 8622-8633.

S18. H. Zhou, T. Yang, Z. Kou, L. Shen, Y. F. Zhao, Z. Wang, X. Wang, Z. Yang, J. Du, J. Xu, M. Chen, L. Tian, W. Guo, Q. Wang, H. Lv, W. Chen, X. Hong, J. Luo, D. He and Y. Wu, *Angew. Chem. Int. Ed.*, 2020, **59**, 20645-20649.

S19. L. Feng, M. Zhou, D. He, H. Yin, Y. Huang, L. Cao, Y. Fang, D. Chu, Y. Liu, H. Chen, G. Li, J. Huang, *Chem. Eng. J.*, 2024, **496**, 154255.

S20. X. Yan, D. Liu, P. Guo, Y. He, X. Wang, Z. Li, H. Pan, D. Sun, F. Fang and R. Wu, *Adv. Mater.*, 2023, **35**, 2210975.